Volume 14
Number 21
7 June 2023
Pages 2535-2654

Polymer Chemistry

rsc.li/polymers

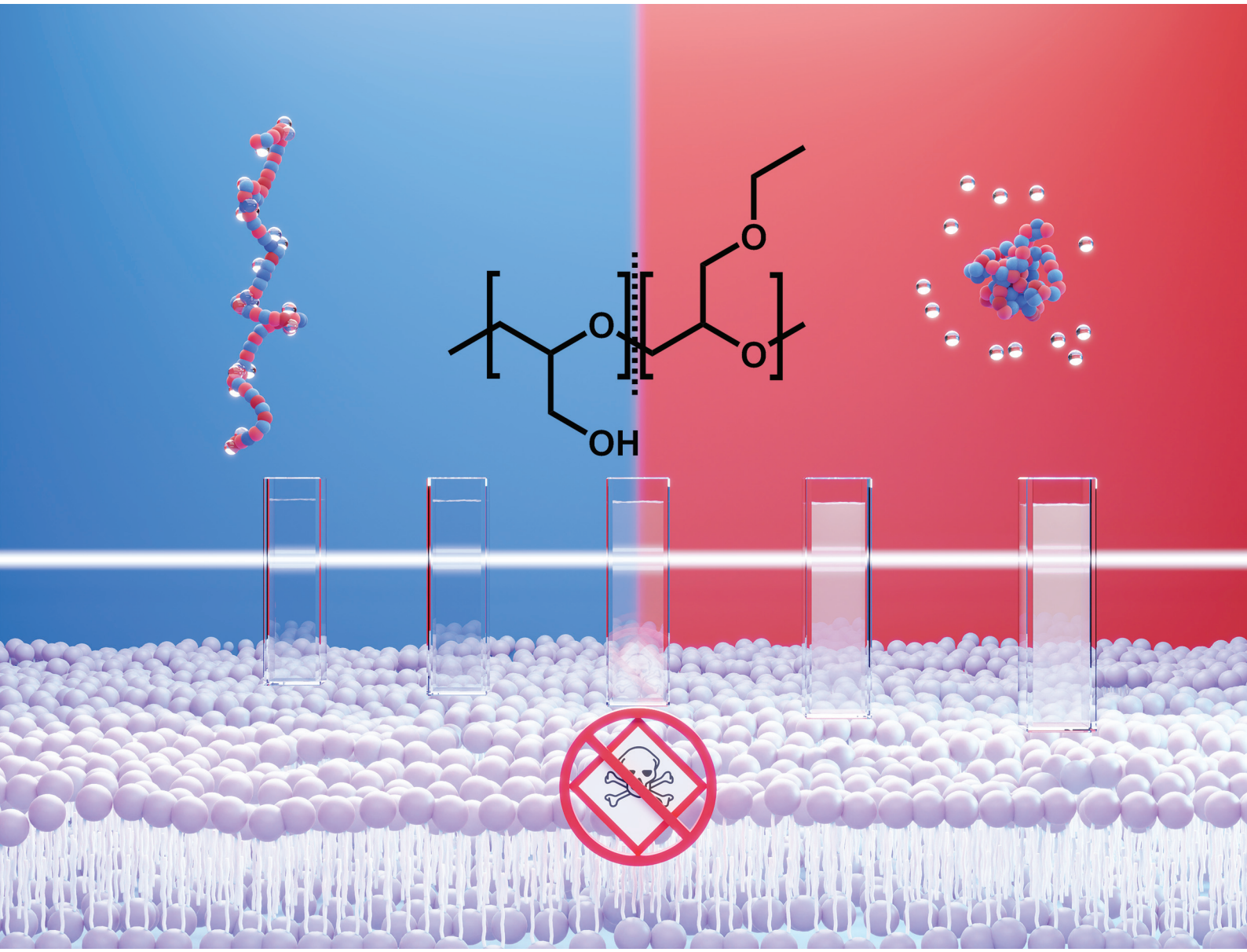

ISSN 1759-9962

ROYAL SOCIETY OF CHEMISTRY

PAPER
Philip Dreier, Holger Frey *et al.*
Tailoring thermoresponsiveness of biocompatible polyethers: copolymers of linear glycerol and ethyl glycidyl ether

Polymer Chemistry

ROYAL SOCIETY OF CHEMISTRY

PAPER

View Article Online
View Journal | View Issue

Cite this: *Polym. Chem.*, 2023, **14**, 2599

Tailoring thermoresponsiveness of biocompatible polyethers: copolymers of linear glycerol and ethyl glycidyl ether†

Verena Müller,[a] Rebecca Matthes,[a] Manfred Wagner,[b] Matthias Bros,[c] Philip Dreier*[a] and Holger Frey*[a]

Linear polyglycerol is known as a highly hydrophilic and biocompatible polymer that is currently considered for numerous medical applications. Derived from this well-known structure, the synthesis of highly biocompatible, thermoresponsive polyether copolymers *via* statistical anionic ring-opening copolymerization of ethyl glycidyl ether (EGE) and ethoxy ethyl glycidyl ether (EEGE) is described. Subsequent deprotection of the acetal groups of EEGE yields copolymers of linear glycerol (*lin*G) and EGE, P(*lin*G-*co*-EGE). These copolymers showed monomodal and narrow molecular weight distributions with dispersities $Đ \leq 1.07$. The microstructure was investigated *via in situ* ^{1}H NMR kinetics experiments, revealing reactivity ratios of $r_{EEGE} = 1.787 \pm 0.007$ and $r_{EGE} = 0.560 \pm 0.002$, showing a slightly favored incorporation of EEGE over EGE. Due to the deliberate incorporation of rather hydrophobic EGE units into the water soluble *lin*PG, tunable thermoresponsive behavior is achieved with cloud point temperatures T_{cp} between 9.0–71.4 °C. Besides the commonly utilized method turbidimetry, temperature-dependent ^{1}H NMR measurements were used for more accurate and reproducible results. The change of the hydrodynamic radii r_H of the copolymers and their aggregates upon reaching T_{cp} was investigated *via* DOSY NMR spectroscopy. To explore possible biomedical applications, as an example, the cell viability and immunology of an exemplary P(*lin*G-*co*-EGE) copolymer sample was investigated. Since both, cell viability and immunology are comparable to the gold standard PEG, the herein presented copolymers show high potential as biocompatible and thermoresponsive alternatives to PEG for biomedical applications.

Received 18th January 2023,
Accepted 17th March 2023

DOI: 10.1039/d3py00064h

rsc.li/polymers

Introduction

Polymers showing responsive behavior to external stimuli, especially thermoresponsive behavior, are promising materials for many applications, *e.g.* drug delivery[1,2] or tissue engineering.[3,4] Thermoresponsive polymers with a lower critical solution temperature (LCST) are water soluble due to strong hydration of the polymer molecules below a critical temperature, the cloud point temperature T_{cp}. Upon temperature increase above the T_{cp}, the polymer chains aggregate due to inter- and intramolecular interaction.[5,6] Thermodynamically, the cloud point phase separation is driven by unfavorable entropy of mixing.[2,4,5]

The most intensely studied thermoresponsive polymer is poly(*N*-isopropylacrylamide) (PNIPAAm), which exhibits LCST behavior with T_{cp} = 32 °C.[7] However, there is a controversial discussion regarding the toxicity of PNIPAAm. Monomer impurities in the polymer can cause cytotoxicity and therefore PNIPAAm has been viewed to be problematic for biomedical applications.[8]

Biocompatible alternatives to PNIPAAm may be found in the polymer class of thermoresponsive polyethers.[9] Generally, aliphatic polyethers can be synthesized *via* anionic ring-opening polymerization (AROP),[10] monomer-activated ring-opening polymerization (MAROP)[11] or AROP with phosphazene bases[12–14] amongst other (organo-)catalytic pathways. The AROP of glycidyl ethers is limited with respect to molecular weights due to proton abstraction in α-position of the epoxide moiety under the harsh, basic polymerization conditions.[15] This side reaction, also known for the AROP of propylene oxide,[10] can be prevented to some extent, if a weakly binding counterion like Cs^+ is utilized in a polar and aprotic solvent at room temperature.[10,16] Nevertheless, to obtain higher molecular weights, both AROP with phosphazene bases and MAROP were introduced. The drawback of both polymerization

[a]*Department of Chemistry, Johannes Gutenberg University, Duesbergweg 10-14, D-55128 Mainz, Germany. E-mail: hfrey@uni-mainz.de*
[b]*Max Planck Institute for Polymer Chemistry, Ackermannweg 10, D-55128 Mainz, Germany*
[c]*University Medical Centre, Johannes Gutenberg University, Langenbeckstraße 1, D-55101 Mainz, Germany*

† Electronic supplementary information (ESI) available. See DOI: https://doi.org/10.1039/d3py00064h

techniques is the demanding work-up procedure and the toxicity of impurities, *i.e.* phosphazene base or inorganic salt, which can cause cytotoxicity of the obtained polymers.[10–13,17] If biomedical applications of polyethers are targeted, AROP is best suited and highly established for medical grade PEG, because no toxic catalyst is required, and highly defined materials are obtained.[18]

Aoki *et al.*[19] investigated the thermoresponsive behavior of poly(glycidyl ether) homopolymers, namely poly(glycidyl methyl ether) (PGME) and poly(ethyl glycidyl ether) (PEGE) *via* turbidimetry and reported a T_{cp} of 57.7 °C and 14.6 °C, respectively. Schmalz *et al.*[20] introduced statistical copolymers of glycidyl methyl ether (GME) and ethyl glycidyl ether (EGE) (P(GME-*co*-EGE)) with T_{cp} between 10 and 58 °C, depending on the copolymer composition. An increase of the amount of the more hydrophilic comonomer GME leads to an increasing T_{cp}. The T_{cp} is not merely dependent on the copolymer composition, but equally on the polymer solution concentration and molecular weight.[21,22] In a detailed study, Weinhart *et al.*[21] synthesized random P(GME-*co*-EGE) copolymers and investigated the effect of increasing concentration and molecular weight on the T_{cp}, both leading to decreased T_{cp}.[5,21] The presence of hydroxy functionalities instead of methoxy or ethoxy groups in each repeating unit results in the homopolymer of glycerol, linear polyglycerol (*lin*PG), which shows very high aqueous solubility and biocompatibility, surpassing even the current gold standard poly(ethylene glycol) (PEG).[23–25] Since direct AROP of the corresponding monomer glycidol leads to hyperbranched polyglycerol, *lin*PG is commonly obtained *via* deprotection of various poly(glycidyl ethers), based on ethoxy ethyl glycidyl ether (EEGE), allyl glycidyl ether (AGE), *tert*-butyl glycidyl ether (*t*BGE) or benzyl glycidyl ether (BnGE).[24,26,27] Due to the presence of the side chains and their atactic nature resulting from the polymerization of racemic monomer mixtures, *lin*PG is obtained as an amorphous material.[24] In contrast, PEG, which is a biocompatible polyether used in medicine and pharmaceutics, possesses no side chains and represents a semi-crystalline polymer.[10,28] As recently shown by Kakuchi *et al.*,[27] the copolymerization of protected glycidol with a more hydrophobic comonomer relying on phosphazene-base promoted AROP can be exploited to tailor the LCST behavior of the resulting copolymers. The authors reported the synthesis of the copolymer P(*lin*G-*co*-EGE) and corresponding (multi)block copolymers. These P(*lin*G-*co*-EGE) copolymers showed thermoresponsive behavior in aqueous solution with T_{cp} values ranging between 30.5 and 70.4 °C, depending on the copolymer composition.

The thermoresponsive behavior of copolymers depends on the copolymer microstructure, which is governed by the polymerization technique. The reactivity ratios of the copolymerization of GME and EGE are very similar, when the polymerization is conducted *via* MAROP (r_{GME} = 0.98 and r_{EGE} = 0.95 (Kelen-Tüdõs method)[21]), albeit very different under AROP conditions (r_{GME} = 1.31 and r_{EGE} = 0.55 (Fineman-Ross method)[20]). The ideally random EGE/GME copolymers prepared *via* MAROP by Weinhart *et al.*[21] exhibit a sharp decrease of transmittance with increasing temperature. In contrast, the decrease of transmission was broadened for copolymers synthesized *via* AROP, which exhibit a soft gradient in the microstructure. As the molecular weights of the copolymers are comparable (M_n = 2200 g mol^{-1} (MAROP) and M_n = 1800 g mol^{-1} (AROP)) and the ratio of EGE : GME is the same (3 : 1), this difference was assigned to the different copolymer microstructure.[21] Kakuchi *et al.*[27] investigated the difference in the thermoresponsive behavior of statistical and (multi)block copolymers of EGE and *lin*G. The statistical copolymer P(*lin*G-*co*-EGE) with an EGE-amount of 60% exhibited thermoresponsive behavior with T_{cp} = 50.5 °C. Both the triblock copolymer P(EGE-*b*-*lin*G-*b*-EGE) and the pentablock copolymer P(EGE-*b*-*lin*G-*b*-EGE-*b*-*lin*G-*b*-EGE) with an EGE amount of 70% and 60%, respectively, showed thermoresponsive behavior with similar cloud points. In contrast, the block copolymer P(*lin*G-*b*-EGE) with an EGE amount of 60% shows a two-step change in transmission. First the transmittance decreases with increasing temperature, before it increases again.

The commonly utilized method for characterization of thermoresponsive behavior is turbidimetry due to its simple implementation in a temperature-controlled UV/Vis spectrometer. The drawback of this method is that measurements can be influenced by multiple factors, *e.g.* heating rate, wavelength, stirring rate and the cuvette.[5] Further, external factors like humidity or air bubbles may also influence the measurements. Other characterization methods for thermoresponsive behavior are dynamic light scattering (DLS),[5,29] differential scanning calorimetry (DSC)[5,30] or ^{1}H NMR spectroscopy.[5,31] The latter detects the thermoresponsive change in structure on a molecular level and is therefore highly precise.[5]

Here we describe the synthesis of thermoresponsive statistical P(*lin*G-*co*-EGE) copolymers *via* AROP of EEGE with EGE and subsequent removal of the acetal protective groups. Since the polymers are intended for biomedical purposes, the use of phosphazene bases is avoided, and "classical" AROP was employed. Molecular weights in the range of 3000 to 4500 g mol^{-1} were targeted, since this molecular weight range is often utilized in biomedical or pharmaceutical applications of PEG.[25] Reactivity ratios are determined *via* precise *in situ* ^{1}H NMR kinetics measurements to elucidate the respective copolymer microstructure. An in-depth comparison of the critical solution behavior studied both *via* turbidimetry and ^{1}H NMR spectroscopy is presented. Since no toxic catalysts or additives are required for the AROP, the synthesized copolymers are promising for biomedical applications. To evidence suitability for this field, the biocompatibility is demonstrated by cell viability and immunology assays with several murine cell types.

Experimental

Materials

All reagents were purchased from TCI, Sigma Aldrich, Acros Organics or VWR and used as received, unless otherwise stated. Ethyl glycidyl ether (EGE) was distilled before use. THF

was flushed through basic Al_2O_3 to remove the stabilizer butylated hydroxytoluene (BHT). The synthesis of ethoxy ethyl glycidyl ether (EEGE) was performed according to a literature synthesis by Fitton *et al.*[32] EGE and EEGE were dried over CaH_2 before all polymerizations. Dowex® was activated with conc. aqueous HCl. Deuterated solvents were purchased from Deutero GmbH.

Instrumentation

^{1}H NMR spectra at 400 MHz and ^{13}C NMR spectra at 100 MHz were recorded on a Bruker Advance II 400 and are referenced internally to residual proton signals of the deuterated solvent. *In situ* ^{1}H NMR kinetics studies were performed at 300 MHz on a Bruker Advance III HD 300, referenced internally to residual proton signals of the deuterated solvent. The graphic representation of the *in situ* ^{1}H NMR kinetics was achieved with NIREVAL software from Steube, Johann, Frey *et al.*[33] For T_{cp} measurements, ^{1}H NMR spectra at 500 MHz were recorded on a Bruker Advance III BR 500/51 and are referenced internally to residual proton signals of the deuterated solvent. The samples were brought to a specific temperature, and this temperature was kept constant for 30 min before a spectrum was measured. After that, the temperature was increased by 1 °C. DOSY measurements were recorded at 500 MHz on a Bruker III BR 500/51. SEC measurements were performed in DMF (flow rate: 1 mL min^{-1}) with the internal standard toluene using an Agilent 1100 series with a HEMA 300/100/40 Å column cascade and RI detector. Calibration was carried out using poly(ethylene glycol) (PEG) standards provided by PSS. Matrix-assisted laser desorption and ionization time-of-flight mass spectroscopy (MALDI-ToF MS) measurements were performed on a Bruker Autoflex Max MALDI-ToF/ToF using *trans*-2-[3-(4-*tert*-butylphenyl)-2-methyl-2-propenyliden]malononitrile (DCTB) or α-cyano-4-hydroxycinnamic acid (HCCA) as a matrix and trifluoroacetic acid potassium salt (KTFA) or lithium chloride (LiCl) as a salt additive. UV/Vis transmittance measurements were performed with a Jasco V-630 UV/Vis spectrometer (λ = 600 nm, quartz cuvette, d = 10 mm). Measurements were performed in Milli-Q water at varying concentrations between 0.1 and 10.0 mg mL^{-1} at heating/cooling rates of 1.0 °C min^{-1}. The normalized transmittance *vs.* temperature curve was fitted *via* sigmoidal fit. The cloud point temperature T_{cp} was defined as the temperature with 50% normalized transmittance.

In situ ^{1}H NMR kinetic studies and determination of reactivity ratios

The pre-dried initiator, the cesium salt of 2-benzyloxyethanol, was dissolved in DMSO-d_6 and an aliquot was added to an NMR tube equipped with a Teflon stopcock. The monomers (24 mol% EEGE, 76 mol% EGE, total: 20 vol-%) were dried over CaH_2 and added at −60 °C to the initiator solution. The solution was heated up to 25 °C right before the NMR measurement. All spectra were measured at 300 MHz with a time interval of 5 min between the spectra. The copolymerization ratios were determined *via* the non-terminal Jaacks method[34] by the decreasing monomer proton signals at 2.70–2.71 ppm (EGE) and 2.74–2.75 ppm (EEGE). More details can be found in the ESI.† Due to the calculated copolymerization parameters, the microstructure of the copolymer was determined using NIREVAL software from Steube, Johann, Frey *et al.*[33]

Investigation of immune cell viability and immunophenotype

Spleens were retrieved from C57BL/6 mice using a 40 μm cell strainer (Greiner Bio-One) to obtain a single cell suspension. Erythrocytes were lysed with a hypotonic lysis buffer. Spleen cells (4×10^6 mL^{-1}) were resuspended in IMDM culture medium supplemented with 5% fetal bovine serum, 100 U mL^{-1} penicillin, 100 μg mL^{-1} streptomycin, 50 μm β-mercaptoethanol and 2 mm L-glutamine and transferred into FACS tubes (500 μL). The copolymer or mPEG (M = 5000 g mol^{-1}) was added (c = 1 and 10 μg mL^{-1}) and samples were incubated overnight. After washing, the samples were incubated with fluorescence-labeled antibodies (CD-11b-SB600, CD11c-BV421, CD19-SB702, CD86-FITC, Ly6G-PE/eFl610, MHCII-APC, NK1.1-PE; all from Biolegend) and FVD-eFl780 (ThermoFisher) to discriminate viable/dead cells. Then, the samples were fixed in PBS containing 2 mm EDTA and 0.7% paraformaldehyde and analyzed in an Attune NxT flow cytometer (ThermoFisher). The spleen cell populations were identified *via* sequential gating.

Synthesis of protected poly(ethoxy ethyl glycidyl ether-*co*-ethyl glycidyl ether) (P(EEGE-*co*-EGE))

General procedure. CsOH·H_2O (0.9 eq.), dissolved in THF/Milli-Q water, and 2-benzyloxyethanol (1.0 eq.), dissolved in benzene, were mixed and the solvents were azeotropically removed at 60 °C. The initiator salt was dissolved in dry DMSO and cooled down to −78 °C. EEGE and EGE were added to the initiator salt solution under high vacuum. The reaction mixture was heated to 25 °C and stirred for at least 24 h. Subsequently, the reaction mixture was dissolved in CH_2Cl_2 and extracted against deionized water (3×) and brine (1×). The organic phase was dried over $MgSO_4$ and the solvent was removed under reduced pressure. The copolymers were obtained as a colourless to light yellow viscous liquid. Yields: 44–99%. ^{1}H NMR (DMSO-d_6, 400 MHz): δ = 7.24–7.36 (m, 5H, H_{arom}), 4.64 (d, OCH(CH$_3$)O), 4.49 (s, 2H, PhCH_2O), 3.38–3.60 (m, polyether backbone), 1.17 (d, OCH(CH_3)O), 1.09 (t, OCH$_2$CH_3) ppm.

Synthesis of deprotected poly(linear glycerol-*co*-ethyl glycidyl ether) (P(*lin*G-*co*-EGE))

General procedure. The corresponding copolymer P(EEGE-*co*-EGE) was dissolved in methanol. The ion exchange resin Dowex® was added to the reaction mixture. The reaction mixture was stirred at 25 °C for at least 20 h before it was filtrated. The filtrate was dried over $MgSO_4$, and the solvent was removed under reduced pressure. The products were obtained as colourless to light yellow viscous liquids. Yields: 72–95%. ^{1}H NMR (DMSO-d_6, 400 MHz): δ = 7.24–7.36 (m, 5H, H_{arom}),

4.45–4.60 (m, PhCH_2O and CH_2OH), 3.29–3.60 (m, polyether backbone), 1.09 (t, OCH_2CH_3) ppm.

Results and discussion

Synthesis of protected poly(ethoxy ethyl glycidyl ether-*co*-ethyl glycidyl ether) (P(EEGE-*co*-EGE)) *via* AROP

The monomer ethoxy ethyl glycidyl ether (EEGE) was synthesized from ethyl vinyl ether and glycidol according to an established protocol.[32] The ^{1}H NMR spectrum of the synthesized EEGE is shown in Fig. S1 (ESI).† For copolymerizations, the initiator 2-benzyloxyethanol was deprotonated with CsOH resulting in a degree of deprotonation of 90%. The copolymers with comonomer ratios between 10 : 90 and 80 : 20 mol% (EEGE : EGE) and the corresponding homopolymers were synthesized at room temperature (25 °C) in DMSO (Scheme 1). These polymerization conditions were crucial to suppress proton abstraction from the glycidyl ethers during polymerization.[10,16] Compilations of all ^{1}H NMR spectra and ^{13}C NMR spectra are shown in Fig. S2 and S3 (ESI),† respectively. All signals can be assigned to the targeted copolymer structure. Importantly, there are no signals of allylic species (δ = 5.5–6.5 ppm), consequently no significant extent of proton abstraction was observed. The degrees of polymerization (X_n) and copolymer compositions are listed in Table 1. The compositions were calculated from the corresponding ^{1}H NMR spectra by comparison of the integrals of the methyl groups (CH_3(5): δ = 1.17 ppm and CH_3(4): δ = 1.19 ppm). The detailed calculation of the composition can be found in the ESI.† The determined compositions are in good agreement with the monomer ratios employed. Small deviations are caused by systematic errors during integration of the ^{1}H NMR spectra.

The molecular weights M_n of the copolymers were determined *via* ^{1}H NMR spectroscopy, SEC and MALDI-ToF MS, the dispersities $Đ$ were determined by SEC. The targeted and determined molecular weights from ^{1}H NMR spectroscopy are in good agreement, showing quantitative consumption of both monomers. The molecular weights determined by SEC are generally underestimated because of the deviating hydrodynamic radii of the copolymers. This is due to the presence of side chains and different polarity compared to the poly(ethylene glycol) (PEG) standards. All samples show narrow and monomodal molecular weight distributions in MALDI-ToF MS (Fig. 1) as well as in SEC (Fig. 2 and Fig. S5, ESI†), confirming the controlled copolymerization under the established polymerization conditions.

In Table 2, molecular weight characterization is presented. The lower M_n observed in MALDI-ToF MS measurements in comparison to ^{1}H NMR measurements may be caused by partial deprotection of the acetal groups during the measurements (see Fig. S6, ESI†).

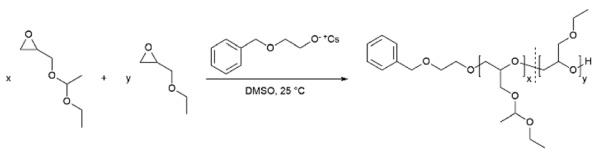

Scheme 1 Synthesis of the copolymers P(EEGE-*co*-EGE) *via* AROP.

Removal of protective groups to poly(linear glycerol-*co*-ethyl glycidyl ether) (P(*lin*G-*co*-EGE))

The acetal protecting group of the EEGE units of the homo- and copolymers were removed *via* acidic deprotection using the ion exchange resin Dowex® (Scheme 2). Successful deprotection was confirmed by ^{1}H NMR spectroscopy, as shown exemplarily for the copolymer P(linG$_{0.57}$-*co*-EGE$_{0.43}$) in Fig. 3.

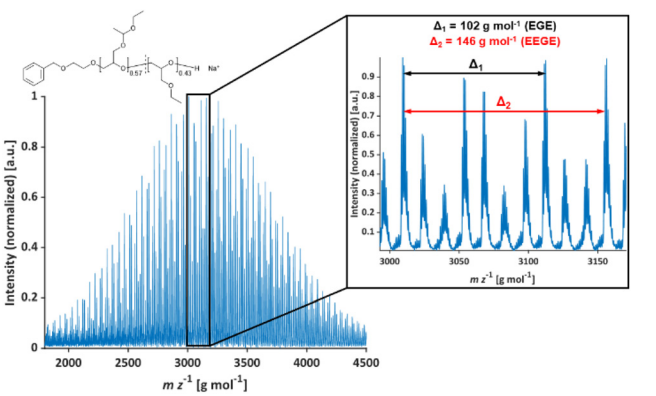

Fig. 1 MALDI-ToF mass spectrum of P(EEGE$_{0.57}$-*co*-EGE$_{0.43}$); matrix: *trans*-2-[3-(4-*tert*-butylphenyl)-2-methyl-2-propenyliden]malononitrile (DCTB), salt additive: trifluoroacetic acid potassium salt (KTFA).

Table 1 Composition of all P(EEGE-*co*-EGE) copolymers and the homopolymers PEGE and PEEGE

	Copolymer	$X_{n,th.}$ (EEGE : EGE)	X_n [a] (EEGE : EGE)	mol% EEGE$_{th.}$	mol% EEGE[a]
1	PEGE	0 : 30	0 : 37	0	0
2	P(EEGE$_{0.9}$-*co*-EGE$_{0.91}$)	3 : 27	3 : 31	10	9
3	P(EEGE$_{0.43}$-*co*-EGE$_{0.57}$)	10 : 15	11 : 14	40	43
4	P(EEGE$_{0.50}$-*co*-EGE$_{0.50}$)	13 : 13	11 : 11	50	50
5	P(EEGE$_{0.57}$-*co*-EGE$_{0.43}$)	18 : 12	18 : 13	60	57
6	P(EEGE$_{0.77}$-*co*-EGE$_{0.23}$)	24 : 6	24 : 7	80	77
7	PEEGE	22 : 0	25 : 0	100	100

[a] Determined by ^{1}H NMR spectroscopy (400 MHz, DMSO-d$_6$).

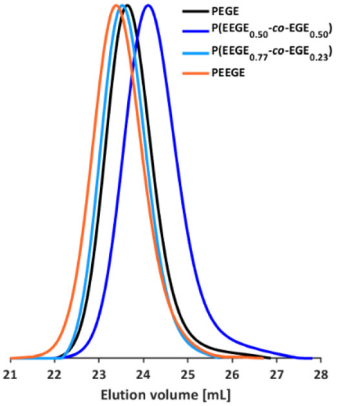

Fig. 2 SEC curves (DMF, PEG calibration) of selected P(EEGE-*co*-EGE) copolymers and the homopolymers PEGE and PEEGE.

The ^{1}H NMR spectrum confirms the absence of acetal protons (δ = 4.64 ppm) and protons of the methyl group next to the acetal group (δ = 1.17 ppm) after deprotection (black spectrum, Fig. 3), indicating the successful cleavage of the protecting groups. Additionally, the signal for the hydroxy group (δ = 4.50 ppm) after deprotection can be assigned to the deprotected *lin*G units. The ^{1}H NMR and ^{13}C NMR spectra for all copolymers are shown in Fig. S7 and S8 (ESI),† respectively.

The molecular weights of the deprotected *lin*PG copolymers were analyzed in analogy to the aforementioned copolymer samples and are in good agreement with the calculated molecular weights. The molecular weight distributions determined by SEC (Fig. 4 and Fig. S9–S10, ESI†) are narrow and monomodal for all samples, with the exception of P(*lin*G$_{0.57}$-*co*-EGE$_{0.43}$). All MALDI-ToF mass spectra show monomodal molecular weight distributions (example in Fig. S11, ESI†). Table 3 compares the investigated molecular weights. Differences of the molecular weights of MALDI-ToF MS analysis compared to the calculated M_n are caused by the determination of the theoretical molecular weights, which is based on the error-prone integration of ^{1}H NMR spectra.

Determination of the reactivity ratios of the monomers EEGE (r_{EEGE}) and EGE (r_{EGE}) polymerized by AROP

To determine the reactivity ratios, the copolymerization of EEGE and EGE was performed in DMSO-d$_6$ inside a NMR tube,

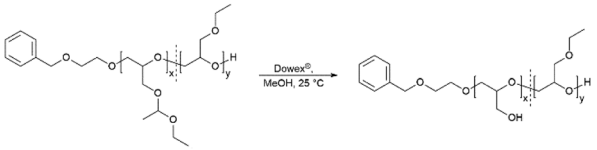

Scheme 2 Synthesis of the copolymers P(*lin*G-*co*-EGE) *via* acidic deprotection with the ion exchange resin Dowex®.

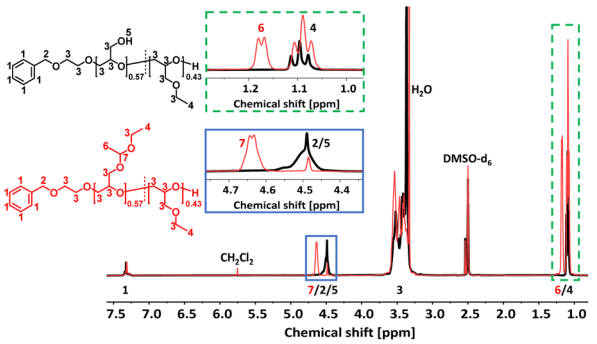

Fig. 3 Stacked ^{1}H NMR spectra (400 MHz, DMSO-d$_6$) of P(*lin*G$_{0.57}$-*co*-EGE$_{0.43}$) (black) and P(EEGE$_{0.57}$-*co*-EGE$_{0.43}$) (red).

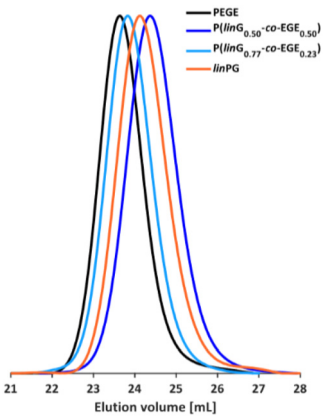

Fig. 4 SEC curves (DMF, PEG calibration) of selected P(*lin*G-*co*-EGE) copolymers and the homopolymers PEGE and *lin*PG.

Table 2 Overview of characterization data of all P(EEGE-*co*-EGE) copolymers and the homopolymers PEGE and PEEGE

	Copolymer	$M_{n,th.}$ [g mol^{-1}]	M_n [a] [g mol^{-1}]	M_n [b] [g mol^{-1}]	M_n [c] [g mol^{-1}]	$Đ$ [b]
1	PEGE	3400	3800	1900	2900	1.05
2	P(EEGE$_{0.9}$-*co*-EGE$_{0.91}$)	3300	3800	2000	3000	1.04
3	P(EEGE$_{0.43}$-*co*-EGE$_{0.57}$)	3100	2900	1700	2700	1.05
4	P(EEGE$_{0.50}$-*co*-EGE$_{0.50}$)	3400	2900	1500	2600	1.08
5	P(EEGE$_{0.57}$-*co*-EGE$_{0.43}$)	4000	4000	2000	3300	1.04
6	P(EEGE$_{0.77}$-*co*-EGE$_{0.23}$)	4300	4400	2000	3400	1.04
7	PEEGE	3500	3800	1800	3100	1.07

[a] Determined by ^{1}H NMR spectroscopy. [b] Determined by SEC. [c] Determined by MALDI-ToF MS.

Table 3 Overview of characterization data of all P(*lin*G-*co*-EGE) copolymers and the homopolymers PEGE and *lin*PG

	Copolymer	$M_{n,th.}$ [a] [g mol^{-1}]	M_n [b] [g mol^{-1}]	M_n [c] [g mol^{-1}]	M_n [d] [g mol^{-1}]	$Đ$ [b]
1	PEGE	3400	3800	1900	2900	1.05
2	P(*lin*G_9-*co*-EGE_{91})	3500	3300	1900	2900	1.06
3	P(*lin*G_{43}-*co*-EGE_{57})	2200	2600	1600	1900	1.07
4	P(*lin*G_{50}-*co*-EGE_{50})	2100	2200	1400	1600	1.07
5	P(*lin*G_{57}-*co*-EGE_{43})	2800	2400	1900	2100	1.12
6	P(*lin*G_{77}-*co*-EGE_{23})	2600	2300	1700	1800	1.06
7	*lin*PG	2000	2200	1500	1600	1.07

[a] Calculated from the composition of P(EEGE-*co*-EGE) copolymers assuming complete deprotection of the acetal protecting groups. [b] Determined by ^{1}H NMR spectroscopy. [c] Determined by SEC. [d] Determined by MALDI-ToF MS.

employing the synthesis conditions described above. For these studies, the targeted composition was 24 mol% EEGE and 76 mol% EGE, respectively. For determination of the reactivity ratios, the consumption of both monomers was followed *via in situ* ^{1}H NMR spectroscopy. Due to similar chemical shifts of the monomer proton signals in the ^{1}H NMR spectrum, the non-overlapping part of one proton of the epoxide methylene group of each monomer is considered exclusively (Fig. S12, ESI†). Fig. 5 (left) shows the consumption of each monomer *vs.* total conversion, demonstrating faster incorporation of EEGE compared to EGE. This is further evaluated by the determination of the reactivity ratios r_1 and r_2. The reactivity ratios are defined by the varying rate constants k_{11}, k_{12}, k_{21} and k_{22} (eqn (1) and (2)).

$$r_1 = \frac{k_{11}}{k_{12}} \quad (1)$$

$$r_2 = \frac{k_{22}}{k_{21}} \quad (2)$$

In non-terminal models, the reactivity ratio r_2 is inversely proportional to r_1 ($r_2 = r_1^{-1}$), relying on the assumption that the reactivity of the chain end is independent of the nature of the active species (EEGE or EGE chain end). As a result, the relative incorporation rate of the monomers is merely dependent on the interaction of the monomer with the counter ion at the chain end.[35,36]

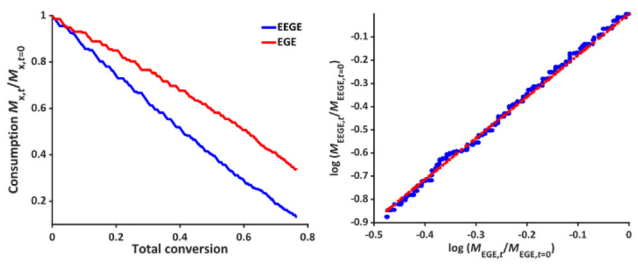

Fig. 5 Left: Monomer consumption $M_{x,t}/M_{x,t\,=\,0}$ *versus* total conversion of P($EEGE_{0.24}$-*co*-$EGE_{0.76}$), determined by *in situ* ^{1}H NMR kinetics study. Right: Logarithmic data fit based on the Jaacks equation to evaluate the reactivity ratios at 25 °C. Blue: Calculated data, red: linear fit. Reactivity ratios: r_{EEGE} = 1.787 ± 0.007, r_{EGE} = 0.560 ± 0.002 with a coefficient of determination R^2 = 0.996.

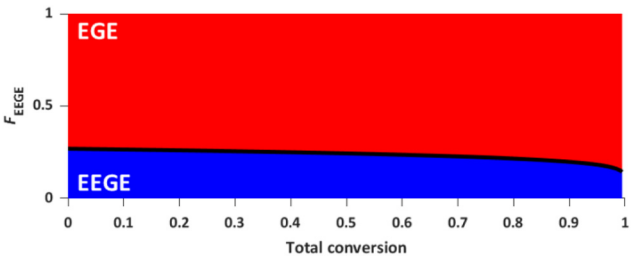

Fig. 6 Monomer fraction *F versus* total conversion of P($EEGE_{0.24}$-*co*-$EGE_{0.76}$).

The reactivity ratios of the copolymerization were calculated by the non-terminal Jaacks approach.[34] From the Jaacks plot (Fig. 5, right), reactivity ratios of r_{EEGE} = 1.787 ± 0.007 and r_{EGE} = 0.560 ± 0.002 are obtained, mirroring a weak gradient microstructure of the copolymer. The microstructure of the copolymer is visualized by plotting the monomer fraction F_{EEGE} *vs.* total conversion (Fig. 6). The slightly preferred incorporation of EEGE over EGE repeating units at the beginning of the copolymerization may be explained by the side chain of EEGE, which contain one additional oxygen atom compared to EGE. In analogy to the recently reported comparison of allyl glycidyl ether and ethoxy vinyl glycidyl ether, one additional oxygen atom increases the chelation capability of the glycidyl ether for the counter cation, leading to a slightly higher reactivity.[35,36]

Lower critical solution temperatures (LCST)

Investigation of the critical solution behavior of P(EEGE-*co*-EGE) *via* turbidimetry. The effect of the hydrophobic, protected comonomer EEGE on the T_{cp} of PEGE was investigated for the copolymer P($EEGE_{0.43}$-*co*-$EGE_{0.57}$) *via* UV/Vis spectroscopy at a wavelength of λ = 600 nm. The temperature dependent transmittance of the polymer solutions in Milli-Q water with concentrations between 0.1 and 10.0 mg mL^{-1} was examined. T_{cp} is defined as the temperature at 50% normalized transmittance, analyzed *via* a sigmoidal fit (sigmoidal function in ESI†). The transmittance *vs.* temperature plots are shown in Fig. 7, and Table 4 compares the determined T_{cp}

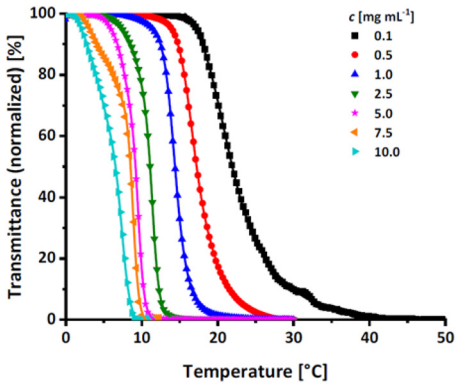

Fig. 7 Transmittance *vs.* temperature plot of the copolymer P(EEGE$_{0.43}$-*co*-EGE$_{0.57}$) at different concentrations. Straight lines show sigmoidal fits to determine T_{cp} at 50% transmittance.

Table 4 Comparison of T_{cp} of the homopolymer PEGE and the acetal-protected copolymer P(EEGE$_{0.43}$-*co*-EGE$_{0.57}$)

	c [mg mL^{-1}]						
	0.1	0.5	1.0	2.5	5.0	7.5	10.0
Polymer	T_{cp} [°C]						
P(EEGE$_{0.43}$-*co*-EGE$_{0.57}$)	21.9	17.2	14.4	11.1	9.2	8.5	6.5
PEGE	27.7	20.4	19.1	15.7	12.0	10.4	9.0

with the homopolymer PEGE (see Fig. S13, ESI†). Due to the more hydrophobic comonomer EEGE, the T_{cp} of the copolymer P(EEGE$_{0.43}$-*co*-EGE$_{0.57}$) is decreased, compared to the T_{cp} of the homopolymer PEGE. The polymer-water interactions are less favored, therefore copolymer aggregation and precipitation occur at lower temperatures.

Investigation of the critical solution behavior of deprotected P(*lin*G-*co*-EGE) *via* turbidimetry. Linear polyglycerol is a highly hydrophilic polymer[24] that shows no change in transmission in the measurable temperature region (see Fig. S14, ESI†). To evaluate the effect of the rather apolar EGE moieties along the chains, the respective T_{cp} of all synthesized P(*lin*G-*co*-EGE) copolymers were determined after removal of the acetal protective groups. Fig. 8 shows the transmittance *vs.* temperature plots upon heating at the example of P(*lin*G$_{0.09}$-*co*-EGE$_{0.91}$). The corresponding plots for copolymers with other compositions (Table 3) are shown in Fig. S15 and S16 (ESI).† Increasing polymer concentration leads to a decrease of T_{cp}. The probability of polymer–polymer interactions increases with concentration, which leads to the favored formation of polymer aggregates at lower temperatures. The change in transmittance is sharp for higher concentrations and is slightly broadened with decreasing concentrations. This is due to a lower local polymer concentration and therefore a more gradual collapse of the polymer chains at lower concentrations.[5]

Fig. S17 (ESI)† compares the heating and cooling curves for the copolymer P(*lin*G$_{0.09}$-*co*-EGE$_{0.91}$) as an example, at a concentration of c = 2.5 mg mL^{-1}. Since the hysteresis is negligibly small, only the heating curves are taken into account hereafter. Table 5 and Fig. 9 summarize the T_{cp} of all P(*lin*G-*co*-EGE)

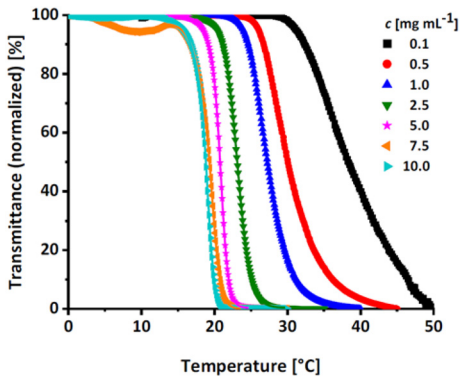

Fig. 8 Transmittance *vs.* temperature plot of the copolymer P(*lin*G$_{0.09}$-*co*-EGE$_{0.91}$) at different concentrations. Straight lines show sigmoidal fits to determine T_{cp} at 50% transmittance.

Table 5 Overview of T_{cp} of all P(*lin*G-*co*-EGE) copolymers and homopolymers in aqueous solution

		c [mg mL^{-1}]						
mol%		0.1	0.5	1.0	2.5	5.0	7.5	10.0
*lin*G		T_{cp} [°C]						
1	0	27.7	20.4	19.1	15.7	12.0	10.4	9.0
2	9	38.3	30.0	27.2	23.1	20.8	19.3	18.8
3	43	—	*	*	*	61.3	57.6	48.5
4	50	—	*	*	*	*	71.4	61.9
5	57	—	—	—	—	—	—	—
6	77	—	—	—	—	—	—	—
7	100	—	—	—	—	—	—	—

— No change in transmittance. * Complete decrease of transmittance not reached at T = 100 °C, T_{cp} cannot be determined.

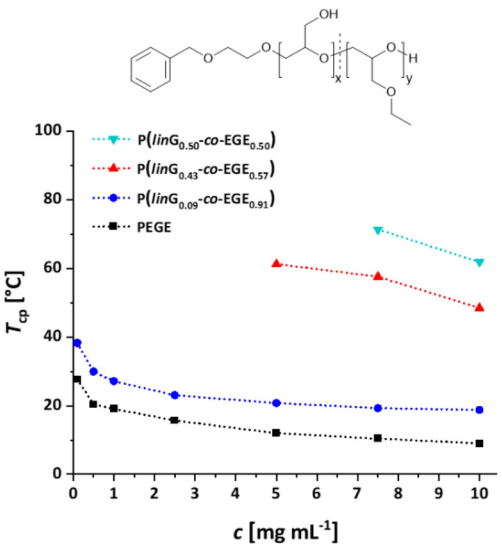

Fig. 9 Summary of concentration dependent T_{cp} of P(*lin*G-*co*-EGE). Dotted lines are depicted to guide the eye.

copolymers and both homopolymers. There is a linear correlation of the content of *lin*G units with the increase of T_{cp}. As expected, an increasing amount of *lin*G units enhances the polarity of the copolymers. Consequently, water-polymer interactions become favored due to hydrogen bonding between water molecules and the hydroxy functionalities. The copolymer with 43% *lin*G units shows no change in transmittance over the whole temperature range for c = 0.1 and an incomplete decrease of transmittance for c = 0.5–2.5 mg mL^{-1}. If the content of *lin*G units exceeds 57%, no T_{cp} was observed for all concentrations.

The described results regarding the thermoresponsive solution behavior of the presented copolymers with *lin*G amounts up to 50% are in line with the recent results of Kakuchi *et al.*[27] These authors synthesized P(*lin*G-*co*-EGE) copolymers *via* a different route, capitalizing on phosphazene base-catalyzed AROP of EGE and benzyl glycidyl ether, followed by deprotection of the benzyl glycidyl ether *via* hydrogenation. However, above a *lin*G amount of 50%, Kakuchi *et al.* still observed T_{cp} values, while our copolymer samples exhibit full solubility up to 100 °C. This may be caused by the higher molecular weights of the copolymers reported by Kakuchi *et al.* (Kakuchi: 11–16 kg mol^{-1}, compared to the herein presented copolymers with 2–4 kg mol^{-1}) and therefore higher local concentration of copolymer in solution. This leads to an earlier aggregation of the copolymers because of a higher possibility for intra- and intermolecular polymer–polymer interactions and thus to a decrease of T_{cp}.[21] Further reasons for the differences in T_{cp} may lie in the microstructure of the copolymers. While the herein presented copolymers exhibit an almost ideally statistical comonomer distribution (Fig. 6), the microstructure of the copolymers of the Kakuchi group was not investigated, but likely deviates from the copolymers of this work due to the different monomer combination and copolymerization technique employed.

Investigation of the critical solution behavior of P(*lin*G-*co*-EGE) *via* ^{1}H NMR spectroscopy. Turbidimetry is a simple and efficient method to determine the critical solution behavior of polymers, but is also sensitive to external influences like humidity or dust impurities. Further, turbidimetry measurements may show a larger systematic error due to other parameters like for example wavelength, cuvette material or stirring rate. Compared to turbidimetry, ^{1}H NMR spectroscopy directly follows the mobility of the polymer chains in solution and mirrors changes in the chemical and electronic environment of the polymer chains. An increase in temperature above T_{cp} and the resulting aggregation of the polymer chains is directly correlated with a decrease in their mobility.[5] Hence, to support the turbidimetry measurements, temperature dependent ^{1}H NMR measurements of the copolymer P(*lin*G$_{0.09}$-*co*-EGE$_{0.91}$) were carried out in D_2O with a concentration of c = 10 mg mL^{-1}. In between each measurement, the temperature was increased by 1 °C. The spectra of P(*lin*G$_{0.09}$-*co*-EGE$_{0.91}$) are shown in Fig. 10. The intensity of the polymer signals starts to decrease upon reaching $T_{cp,NMR}$ = 19 °C as a result of chain aggregation. The mobility of these aggregates is strongly

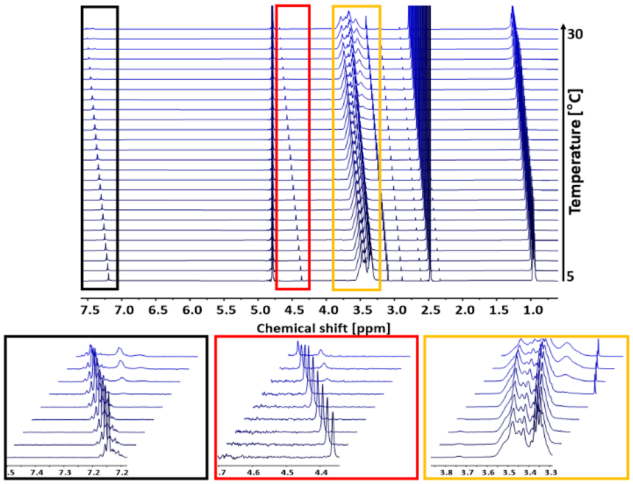

Fig. 10 ^{1}H NMR analysis (500 MHz, D_2O) of T_{cp} of the copolymer P(*lin*G$_{0.09}$-*co*-EGE$_{0.91}$) in a temperature range of 5–30 °C. Insets: Every third spectrum is shown for overview purposes.

lowered compared to the free polymer chains. This decreases the transversal relaxation time T_2, which leads to a broadening of the signals.[37] Additionally, new signals occur at $T_{cp,NMR}$ with chemical shifts to lower fields (see Fig. 10, insets). These new signals are ascribed to the structural change during the aggregation, because the electronic environment of the protons of the polymer chains changes.

In the following, $T_{cp,NMR}$ defines the temperature at which polymer chains start to aggregate. To compare the results of the ^{1}H NMR measurements with the turbidimetry experiment, $T_{cp,UV/VIS}$ is herein defined as the temperature with 95% transmittance because this value marks the beginning of polymer chain aggregation. Compared to $T_{cp,NMR}$ = 19 °C, $T_{cp,UV/Vis}$ has a slightly lower value ($T_{cp,UV/Vis}$ = 15.7 °C). This difference is possibly caused by applying different heating rates for each measurement. While the temperature was increased constantly with a heating rate of 1 °C min^{-1} in the turbidimetry measurement, the temperature in the ^{1}H NMR analysis was kept constant for 30 min before each measurement. Hence, thermodynamic equilibrium between the free polymer chains and the polymer aggregates is established. Considering the precise and constant temperature setting as well as the less systematic error-prone set-up of the ^{1}H NMR compared to UV/Vis analysis, the evaluation *via* NMR constitutes the preferable method leading to more reliable results for the determination of T_{cp}.

Determination of the hydrodynamic radius r_H of P(*lin*G-*co*-EGE) *via* DOSY. To verify aggregation of the copolymer P(*lin*G-*co*-EGE) above T_{cp}, the hydrodynamic radius of the copolymer P(*lin*G$_{0.09}$-*co*-EGE$_{0.91}$) and its aggregates was determined by DOSY NMR for both $T < T_{cp}$ and $T > T_{cp}$ *via* the Stokes–Einstein equation (eqn (3)):[38]

$$D_{DOSY} = \frac{k_B T}{6\pi \cdot \rho(D_2O) \cdot r_H} \quad (3)$$

where D_{DOSY} is the diffusion coefficient determined *via* DOSY, k_b is the Boltzmann constant and $\rho(D_2O)$ is the viscosity of

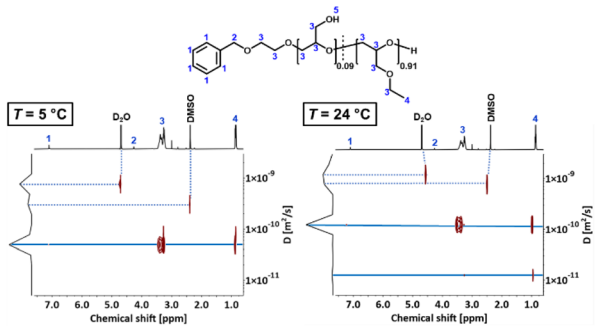

Fig. 11 DOSY spectra of P(*lin*$G_{0.09}$-*co*-$EGE_{0.91}$) at T = 5 °C ($T < T_{cp}$) and 24 °C ($T > T_{cp}$).

Table 6 Overview of diffusion coefficients and hydrodynamic radii of P(*lin*$G_{0.09}$-*co*-$EGE_{0.91}$) for $T < T_{cp}$ and $T > T_{cp}$. Viscosities $\rho(D_2O)$ were taken from literature[39]

T [°C]	D [10^{-11} m^2 s^{-1}]	$\rho(D_2O)$ [mPas]	r_H [nm]
5 ($T < T_{cp}$)	4.882	1.988	2.1
24 ($T > T_{cp}$)	12.337	1.100[a]	1.6
	1.236	1.100[a]	16.0

[a] Viscosity of D_2O for T = 25 °C.[39]

D_2O at the measured temperature. The DOSY spectra for $T < T_{cp}$ and $T > T_{cp}$ are shown in Fig. 11, the corresponding diffusion coefficients and calculated hydrodynamic radii are listed in Table 6. If the temperature is below T_{cp}, a single diffusion coefficient is detected, resulting in a corresponding hydrodynamic radius r_H of 2.1 nm. Above T_{cp}, a second diffusion coefficient appears, which indicates that a fraction of the polymer chains already aggregates, while other parts remain dissolved in solution. The calculated hydrodynamic radii are r_H = 1.6 and 16.0 nm. The species with r_H = 1.6 nm relates to the dissolved copolymer chains in solution. The hydrodynamic radius decreases compared to the hydrodynamic radius at $T < T_{cp}$. Above the cloud point temperatures, polymer–polymer interactions are preferred regarding an increase of entropy. Therefore, the copolymer collapses to reduce the interface to D_2O. The second hydrodynamic radius (r_H = 16.0 nm) indicates polymer aggregates which are formed once T_{cp} is reached.

Immune cell viability and immunophenotype of P(*lin*G-*co*-EGE)

Both *lin*PG and copolymers of short chain alkyl glycidyl ethers (SCAGEs), *e.g.* copolymers of EGE and glycidyl methyl ether (GME) P(EGE-*co*-GME), are known for their excellent biocompatibility and high cell viability.[24,40] To explore potential biomedical applications of the herein synthesized copolymer series P(*lin*G-*co*-EGE), the cell viability and effects of the synthesized copolymer sample P(*lin*$G_{0.57}$-*co*-$EGE_{0.43}$) as a typical representative of the copolyether series on immune cells were explored. For this purpose, the copolymer and monomethyl poly(ethylene glycol) (mPEG) (M_n = 5000 g mol^{-1}) as a reference were incubated with murine cells (c = 1 and 10 μg mL^{-1}) over night. The cell viability was investigated *via* fluorescence-activated cell sorting (FACS) for the following cell types: B cells, natural killer cells (NK), macrophages (Fig. 12, top), dendritic cells (DC), polymorphonuclear cells (PMN) and T cells (Fig. S18, top, ESI†). The copolymer P(*lin*$G_{0.57}$-*co*-$EGE_{0.43}$) shows comparable cell viability as the gold standard mPEG for all cell types for both concentrations, even at a higher concentration of c = 10 μg mL^{-1}. Immunological behavior was investigated by expression of the surface proteins CD80 (Fig. 12, bottom and Fig. S18,† bottom), CD86 and MCHII (both Fig. S19, ESI†). The corresponding fluorescence labelled antibodies of these surface activation markers were measured by FACS. For all cell types, the immune cell activation of the copolymer is comparable to mPEG, independent of the investigated polymer concentration range. Hence, the results indicate the suitability of the presented copolymers for biomedical and pharmaceutical applications as a thermoresponsive alternative to mPEG.

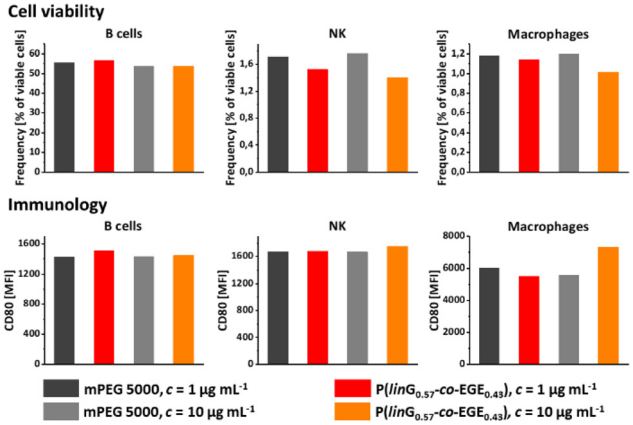

Fig. 12 Cell viability (top) and immunology using the surface protein CD80 (MFI = mean fluorescence intensity) (bottom) of P(*lin*$G_{0.57}$-*co*-$EGE_{0.43}$) and mPEG (M_n = 5000 g mol^{-1}) as a reference for B cells, natural killer cells (NK) and macrophages.

Conclusions

Statistical copolymers of ethyl glycidyl ether (EGE) and linear glycerol (*lin*G) with systematically varied comonomer composition have been prepared. For this purpose, EGE and ethoxy ethyl glycidyl ether (EEGE) were copolymerized *via* anionic ring-opening polymerization (AROP) at room temperature and subsequent acidic deprotection of the acetal group of EEGE. Molecular weights in the range of 2200 to 3800 g mol^{-1} were targeted and confirmed *via* ^{1}H NMR spectroscopy and MALDI ToF MS. The use of catalysts or monomer-activation was avoided to generate copolymers suitable for medical applications. SEC traces of both homopolymers (*lin*PG and PEGE) and copolymers (P(*lin*G_x-*co*-EGE_{1-x}), x: mol% *lin*G) showed

very narrow, monomodal distributions ($Đ$ = 1.04–1.07), confirming controlled homo- and copolymerization, respectively. The copolymerization kinetics of EGE and EEGE was investigated *via in situ* ^{1}H NMR kinetics measurements. Evaluation with the non-terminal Jaacks method resulted in reactivity ratios of r_{EEGE} = 1.787 ± 0.007 and r_{EGE} = 0.560 ± 0.002, confirming a slightly faster incorporation of EEGE over EGE in the polymer chains during AROP. These values show a slight gradient, evidencing an almost ideally random copolymer formation. Further, the thermoresponsive behavior of one exemplary P(EEGE-*co*-EGE) copolymer and all deprotected P(*lin*G-*co*-EGE) copolymers and homopolymers in aqueous solution was investigated *via* turbidimetry. Depending on the polarity (acetal or hydroxymethylene group) and the incorporated amount of side chains, the hydrophilicity of the copolymers can be tailored in a linear fashion. The T_{cp} of the copolymer P(*lin*$G_{0.09}$-*co*-$EGE_{0.91}$) was further investigated *via* temperature-dependent ^{1}H NMR spectroscopy. Compared to the T_{cp} determined *via* turbidimetry, the T_{cp} of the ^{1}H NMR measurements is slightly higher (ΔT_{cp} = 3 °C). This discrepancy might be caused by different heating rates and a less error-prone set-up of the ^{1}H NMR measurement. In addition, the hydrodynamic radius r_H of the copolymer P(*lin*$G_{0.09}$-*co*-$EGE_{0.91}$) was investigated *via* DOSY NMR spectroscopy for both $T < T_{cp}$ and $T > T_{cp}$. For $T < T_{cp}$ merely one species with r_H = 2.1 nm is observed. Above T_{cp}, a second mode with a larger r_H of 16.0 nm appears, which can be assigned to aggregated copolymer chains. Cell viability and immunology of the synthesized copolymers were investigated for P(*lin*$G_{0.77}$-*co*-$EGE_{0.23}$) as a typical copolymer sample. Both cell viability and immunological properties are fully comparable to mPEG, the gold standard polyether broadly used in medicine and pharmaceutics.[28] The herein presented copolymers are therefore suitable as a thermoresponsive alternative for mPEG in (bio)medical applications, permitting to tailor the LCST, *e.g.*, for nanomedicine and thermoresponsive therapeutics.

Author contributions

The manuscript was written through contributions of all authors. All authors have given approval to the final version of the manuscript.

Ethical statement

C57BL/6 mice were kept in the Central Animal Facility of the Johannes Gutenberg-University Mainz under pathogen-free conditions on a standard diet according to the guidelines of the regional animal care committee (Rhineland-Palatinate, Germany). The "Principles of Laboratory Animal Care" (NIH publication no. 85-23, revised 1985) were followed. Ethical review and approval were waived for this study due to exclusive use of isolated mouse cells derived from mice sacrificed for organ retrieval according to § 4(3) TierSchG.

Conflicts of interest

There are no conflicts to declare.

Acknowledgements

V. M. thanks Monika Schmelzer for the SEC measurements and Elena Berger-Nicoletti for the MALDI-ToF MS measurements. H. F., R. M. and P. D. thank the ERC for important financial support in the context of the ERC Advanced Grant "RandoPEGMed".

References

1 (*a*) K. B. Doorty, T. A. Golubeva, A. V. Gorelov, Y. A. Rochev, L. T. Allen, K. A. Dawson, W. M. Gallagher and A. K. Keenan, *Cardiovasc. Pathol.*, 2003, **12**, 105–110; (*b*) H. Vihola, A. Laukkanen, H. Tenhu and J. Hirvonen, *J. Pharm. Sci.*, 2008, **97**, 4783–4793.
2 D. C. Tuncaboylu and C. Wischke, *Pharmaceutics*, 2022, **14**, 2331–2371.
3 R. A. Stile and K. E. Healy, *Biomacromolecules*, 2001, **2**, 185–194.
4 F. Doberenz, K. Zeng, C. Willems, K. Zhang and T. Groth, *J. Mater. Chem. B*, 2020, **8**, 607–628.
5 Q. Zhang, C. Weber, U. S. Schubert and R. Hoogenboom, *Mater. Horiz.*, 2017, **4**, 109–116.
6 H. G. Schild, *Prog. Polym. Sci.*, 1992, **17**, 163–249.
7 S. Fujishige, K. Kubota and I. Ando, *J. Phys. Chem.*, 1989, **93**, 3311–3313.
8 S. Yogev, A. Shabtay-Orbach, A. Nyska and B. Mizrahi, *Toxicol. Pathol.*, 2019, **47**, 426–432.
9 C. Mangold, B. Obermeier, F. Wurm and H. Frey, *Macromol. Rapid Commun.*, 2011, **32**, 1930–1934.
10 J. Herzberger, K. Niederer, H. Pohlit, J. Seiwert, M. Worm, F. R. Wurm and H. Frey, *Chem. Rev.*, 2016, **116**, 2170–2243.
11 C. Billouard, S. Carlotti, P. Desbois and A. Deffieux, *Macromolecules*, 2004, **37**, 4038–4043.
12 B. Eßwein, A. Molenberg and M. Möller, *Macromol. Symp.*, 1996, **107**, 331–340.
13 B. Eßwein, N. M. Steidl and M. Möller, *Macromol. Rapid Commun.*, 1996, **17**, 143–148.
14 (*a*) S. Liu, L. Liu, Y. Zhou, Y. Chen and J. Zhao, *Polym. Chem.*, 2022, **13**, 3650–3659; (*b*) Y. Chen, J. Shen, S. Liu, J. Zhao, Y. Wang and G. Zhang, *Macromolecules*, 2018, **51**, 8286–8297.
15 C. C. Price, Y. Atarashi and R. Yamamoto, *J. Polym. Sci., Part A: Polym. Chem.*, 1969, **7**, 569–574.
16 M. Hans, H. Keul and M. Moeller, *Polymer*, 2009, **50**, 1103–1108.
17 A. Labbé, S. Carlotti, C. Billouard, P. Desbois and A. Deffieux, *Macromolecules*, 2007, **40**, 7842–7847.
18 R. Matthes and H. Frey, *Biomacromolecules*, 2022, **23**, 2219–2235.

19 S. Aoki, A. Koide, S.-I. Imabayashi and M. Watanabe, *Chem. Lett.*, 2002, **31**, 1128–1129.
20 S. Reinicke, J. Schmelz, A. Lapp, M. Karg, T. Hellweg and H. Schmalz, *Soft Matter*, 2009, 2648–2657.
21 S. Heinen, S. Rackow, A. Schäfer and M. Weinhart, *Macromolecules*, 2017, **50**, 44–53.
22 T. Becherer, S. Heinen, Q. Wei, R. Haag and M. Weinhart, *Acta Biomater.*, 2015, **25**, 43–55.
23 (*a*) R. K. Kainthan, J. Janzen, E. Levin, D. V. Devine and D. E. Brooks, *Biomacromolecules*, 2006, **7**, 703–709; (*b*) C. Mangold, F. Wurm, B. Obermeier and H. Frey, *Macromol. Rapid Commun.*, 2010, **31**, 258–264; (*c*) Y. Li, J. Xu and L. Hu, *J. Mol. Liq.*, 2022, **360**, 119538.
24 A. Thomas, S. S. Müller and H. Frey, *Biomacromolecules*, 2014, **15**, 1935–1954.
25 D. Braatz, M. Cherri, M. Tully, M. Dimde, G. Ma, E. Mohammadifar, F. Reisbeck, V. Ahmadi, M. Schirner and R. Haag, *Angew. Chem., Int. Ed.*, 2022, **61**, e202203942.
26 (*a*) M. Erberich, H. Keul and M. Möller, *Macromolecules*, 2007, **40**, 3070–3079; (*b*) K. Knop, R. Hoogenboom, D. Fischer and U. S. Schubert, *Angew. Chem., Int. Ed.*, 2010, **49**, 6288–6308.
27 T. He, Y. Wang, A. Narumi, L. Xu, S.-I. Sato, X. Shen and T. Kakuchi, *Polymers*, 2021, **13**, 3873–3888.
28 C. Fruijtier-Pölloth, *Toxicology*, 2005, **214**, 1–38.
29 (*a*) S. Monge, S. Antoniacomi, V. Lapinte, V. Darcos and J.-J. Robin, *Polym. Chem.*, 2012, **3**, 2502; (*b*) J.-F. Lutz, K. Weichenhan, Ö. Akdemir and A. Hoth, *Macromolecules*, 2007, **40**, 2503–2508.
30 (*a*) M. Karesoja, E. Karjalainen, S. Hietala and H. Tenhu, *J. Phys. Chem. B*, 2014, **118**, 10776–10784; (*b*) A. Laukkanen, L. Valtola, F. M. Winnik and H. Tenhu, *Polymer*, 2005, **46**, 7055–7065.
31 (*a*) T. Li, H. Tang and P. Wu, *Soft Matter*, 2015, **11**, 3046–3055; (*b*) M. V. Deshmukh, A. A. Vaidya, M. G. Kulkarni, P. R. Rajamohanan and S. Ganapathy, *Polymer*, 2000, **41**, 7951–7960.
32 A. O. Fitton, J. Hill, D. E. Jane and R. Millar, *Synthesis*, 1987, 1140–1142.
33 M. Steube, T. Johann, M. Plank, S. Tjaberings, A. H. Gröschel, M. Gallei, H. Frey and A. H. E. Müller, *Macromolecules*, 2019, **52**, 9299–9310.
34 V. Jaacks, *Makromol. Chem.*, 1972, **161**, 161–172.
35 P. Dreier, R. Matthes, R. D. Barent, S. Schüttner, A. H. E. Müller and H. Frey, *Macromol. Chem. Phys.*, 2022, 2200209.
36 B. F. Lee, M. Wolffs, K. T. Delaney, J. K. Sprafke, F. A. Leibfarth, C. J. Hawker and N. A. Lynd, *Macromolecules*, 2012, **45**, 3722–3731.
37 T. Kurotu, *Polym. J.*, 1986, **18**, 859–864.
38 (*a*) G. Stokes, *Trans. Cambridge Philos. Soc.*, 1856, **9**, 5; (*b*) A. Einstein, *Ann. Phys.*, 1905, **17**, 549–560.
39 C. H. Cho, J. Urquidi, S. Singh and G. W. Robinson, *J. Phys. Chem. B*, 1999, **103**, 1991–1994.
40 (*a*) M. Weinhart, I. Grunwald, M. Wyszogrodzka, L. Gaetjen, A. Hartwig and R. Haag, *Chem. – Asian J.*, 2010, **5**, 1992–2000; (*b*) M. Weinhart, T. Becherer and R. Haag, *Chem. Commun.*, 2011, **47**, 1553–1555.